JOURNAL OF STRUCTURAL BIOLOGY 113, 35–46 (1994)

A Structure for the Signal Sequence Binding Protein SRP54: 3D Reconstruction from STEM Images of Single Molecules

GREGORY J. CZARNOTA,* DAVID W. ANDREWS,† NEIL A. FARROW,*,‡ AND F. P. OTTENSMEYER*

*Ontario Cancer Institute and Department of Medical Biophysics, University of Toronto, 500 Sherbourne Street, Toronto, Ontario, M4X 1K9 Canada; †Department of Biochemistry, McMaster University, 1200 Main Street West, Hamilton, Ontario, L8N 3Z5 Canada; and ‡Department of Medical Genetics, University of Toronto, Medical Sciences Building, King's College Circle, Toronto, Ontario, M5S 1A8 Canada

Received July 8, 1994, and in revised form August 17, 1994

The 54-kDa subunit SRP54 of the signal recognition particle in eukaryotic cells is responsible for the recognition of nascent proteins destined for secretion or membrane integration. The three-dimensional structure of this protein was determined using computational techniques applied to images of the molecule obtained via high-resolution, low-dose, scanning transmission electron microscopy at low temperature. The reconstructions at spatial resolutions between 12 and 15 Å feature two unequal domains joined by a slender linker. The two-domain structure is in agreement with genetic and biochemical data indicating organization of SRP54 into a larger N-terminal GTP-binding region and a smaller C-terminal peptide-binding region. The structure has similarities to other protein domains with related functions and similar amino acid sequences. The larger domain of the 3D reconstruction is consistent in shape and size with the GTP-binding domains of EF-Tu and p21-RAS, while the smaller domain is compatible in structure with part of the peptide-binding protein calmodulin. The overall shape of SRP54 and the deduced location of critical functional regions of the molecule provide a structural framework for its known biochemical properties in the targeting cycle of the signal recognition particle.

INTRODUCTION

The 54-kDa protein SRP54 is one of the key components in the protein targeting pathway, recognizing proteins destined for secretion from the cell or for integration into the cell membrane. It is part of the signal recognition particle (SRP), an 11S ribonucleoprotein consisting of six distinct polypeptides (M_r 72 000, 68 000, 54 000, 19 000, 14 000, and 9000) (Walter and Lingappa, 1986) and one molecule of RNA (300 nucleotides, termed 7SL RNA or SRP RNA) (Kurzchalia *et al.*, 1986). SRP has been shown to function as the cellular adapter between the cytoplasmic protein-synthetic apparatus and the membrane associated protein-translocation machinery of the endoplasmic reticulum (Krieg *et al.*, 1986; Gilmore *et al.*, 1982a, b; Meyer *et al.*, 1982; Zopf *et al.*, 1990; Römisch *et al.*, 1990). Complete understanding of this complex system requires not only the elucidation of the series of events in the process, but also knowledge of the function, composition, and structure of the constituent macromolecular complexes. We have shown previously that the entire 300-kDa complex of SRP is a tripartite rod-shaped structure about 23–24 nm in length and 5–6 nm in width using various methods in electron microscopy including negative staining, platinum shadowing, and dark-field imaging of unstained specimens via high-dose transmission electron microscopy (TEM) and via low-dose scanning transmission electron microscopy (STEM) (Andrews *et al.*, 1985, 1987). Phosphorus-specific electron spectroscopic imaging was used to indicate that the SRP RNA molecule traversed the entire length of the particle (Andrews *et al.*, 1987). Here we describe the 3D structure of the signal sequence recognition component of the SRP complex, SRP54, determined using low-dose low-temperature STEM micrographs and a 3D reconstruction approach that permits the use of images of individual randomly oriented molecules.

SRP54 recognizes and binds to the signal sequences of nascent secretory and membrane-integrated proteins. It also binds to the SRP RNA (Krieg *et al.*, 1986; Kurzchalia *et al.*, 1986), the interaction being stabilized by SRP19 (Siegel and Walter, 1985). Genetically and functionally SRP54 consists of two separable domains: a 33-kDa amino-terminal domain with GTP-binding activity (G-domain) and a 22-kDa methionine-rich carboxy-terminal domain (M-domain) within which binding sites for signal sequence and SRP RNA are located (Zopf *et al.*, 1990; Römisch *et al.*, 1990; High and

1047-8477/94 $6.00

Dobberstein, 1991; Samuelsson and Olsson, 1993). The G- and M-domains exhibit homology to other GTP-binding and peptide binding proteins, respectively (Zopf *et al.*, 1990; Römisch *et al.*, 1990; this work). The action of SRP can be considered as a multistage cycle. In brief, SRP54 recognizes and binds to a signal sequence in a nascent peptide emerging from the ribosomal machinery. Peptide synthesis is arrested or slowed and the protein-synthetic complex including SRP is targeted to a membrane-bound receptor. Here the block of peptide synthesis is released and the nascent peptide is fed into or through the membrane (Römisch *et al.*, 1990; High and Dobberstein, 1991). SRP is then released and redirected to monitor new nascent peptides (Walter and Lingappa, 1986; Miller *et al.*, 1993). Miller *et al.* (1993) show that signal-sequence binding and both GTP and GDP binding to SRP54 are mutually exclusive. Furthermore GTP-binding to SRP54 is promoted by interaction of the SRP signal sequence complex and its membrane receptor, with the release of the bound signal sequence. Subsequent hydrolysis of the bound GTP to GDP in the presence of the receptor is required to release SRP from the membrane receptor and return the particle to the cytosol. Binding of GDP to SRP54 is weak (Miller *et al.*, 1993), suggesting that SRP54 is ligand-free when monitoring for potential signal sequences.

The data implies the existence of at least four possible structural states for SRP54: free of bound ligands, signal-sequence-bound, GTP-bound, and GDP-bound. As a starting analysis, the 3D structure determined here is that of SRP54 free of ligands.

3D Approaches in Electron Microscopy

Structure determination of macromolecules via electron microscopy has been most useful when 3D crystals of the specimens have not been available. A number of macromolecular specimens have naturally formed thin two-dimensional crystals or have been induced to crystallize in this form. Such macromolecules have so far produced the best 3D structures by electron microscopy and electron diffraction, with resolutions as good as 3.4 Å for bacteriorhodopsin and the plant light-harvesting complex (Unwin and Henderson, 1976; Henderson *et al.*, 1990; Kühlbrandt *et al.*, 1994). SRP54 has not yet yielded to this approach. For macromolecular assemblies exhibiting other symmetry patterns, modification of crystallographic processing has resulted in 3D structures with detail as fine as 9 Å for the acetylcholine receptor (Unwin, 1993), although for icosahedral viruses about 30 Å detail is more usual (Stewart *et al.*, 1991, 1993).

For individual macromolecules there are few available techniques of 3D reconstruction. Multiple-exposure tilt-series approaches, possible for 2D crystals, exact a prohibitive price in radiation damage when imaging isolated noncrystallized macromolecules. The optimum dose, a single exposure, has been used in the elegant technique of random conical reconstruction for individual molecules distributed on their support film in one or a few preferred orientations (Radermacher *et al.*, 1987; Frank *et al.*, 1988). For isolated molecules with random orientations we have developed a processing algorithm that permits 3D reconstruction from their micrographs (Farrow and Ottensmeyer, 1992, 1993; Ottensmeyer and Farrow, 1992) using the principle of the common axis theorem, sinogram correlation functions, and quaternion vector mathematics for optimum orientation determination among noisy images (Crowther, 1971; van Heel, 1987; Horn, 1987; Harauz, 1990). Another orientation algorithm based on Radon transforms, newly developed by Radermacher (1994), has not yet been applied by us. In tests our algorithm was robust even with the addition of noise to images derived from the known crystal structure of the 68-kDa Klenow fragment of DNA polymerase (Farrow and Ottensmeyer, 1992, 1993). It was also successful in the 3D reconstruction of the structure of this polymerase using micrographs obtained by dark-field TEM (Ottensmeyer and Farrow, 1992), although limited in resolution to about 20 Å by the high dose required by that EM technique.

Following up on the potential realized on the known structure of the polymerase above, SRP54 is the first unknown structure determined by this approach. A major improvement on the method was the use of low-dose STEM micrographs of the freeze-dried protein imaged at low temperatures. The result is a reproducible two-domain structure consistent with biochemical and genetic analyses. The structures of the individual domains exhibit strong correlations with proteins of similar function and with amino acid sequence homology to SRP54. Moreover, the structure is readily incorporated as a model in the cycle of SRP action.

MATERIALS AND METHODS

Biological materials. Purified SRP54 used to initiate this study was obtained as a gift from P. Walter. The purification process is described in Walter and Blobel (1983). It results in a chromatographically pure, ligand-free protein. In this protocol SRP54 is purified in the absence of added guanine nucleotides. Bound peptides, protein, and RNA are separated after dissociation during the high salt extraction from microsomal membranes. Bound GTP and GDP dissociate from SRP54 due to their high k_D values (Miller *et al.*, 1993).

Electron microscopy and image analysis. Purified SRP54 was spread on 30-Å-thin carbon films, quick-frozen after an ammonium acetate wash, freeze-dried, and imaged without contrast agents at liquid nitrogen temperature with the Brookhaven National Laboratory scanning transmission electron microscope equipped with a field-emission gun operating at 80 kV. Quick-freezing to liquid nitrogen temperatures assures immobilization of the molecules in a solid glass-like environment similar to the

aqueous state, while freeze-drying results in a contrast-rich specimen that has not been distorted structurally by phase boundary forces during dehydration. Dark-field electron micrographs of single-particle spreads of molecules were acquired digitally with 5-Å pixel steps at a dose between 20 and 30 e/Å^2, corresponding at this low temperature to an optimal dose for imaging at a resolution of 10 Å (Hayward and Glaeser, 1979). Separate signals from electrons scattered at low angles and at high angles were recorded simultaneously. These were combined during image processing to increase the signal-to-noise ratio. Molecular images of SRP54 were selected automatically based on their relative molecular mass in comparison to TMV as described in Andrews *et al.* (1986).

Mass measurements, using tobacco mosaic virus (TMV) as an internal mass standard, were carried out as described by Wall and Hainfeld (1986).

3D reconstructions. Three-dimensional reconstructions were computed from images of randomly oriented SRP54 molecules via the iterative quaternion-assisted angular determination method (Farrow and Ottensmeyer, 1992, 1993) based on sinogram correlation and the common axis theorem (van Heel, 1987). Calculations were carried out on a μVaxII or a Vax WorkStation 3100 M38 (Digital Equipment Corporation, Maynard, MA). Reconstructions from different sets of images (100, 100, and 200 images) were calculated independently in order to ascertain the degree of reproducibility. After initial interactive alignment of the reconstructions, followed by computer-assisted rotational searches for maximum overlap, three-dimensional correlation coefficients were calculated essentially as described by Penchek *et al.* (1992). Measures of resolution for reconstructions were calculated by computing 3D Fourier transforms for each of the reconstructions and calculating the average differences in phase between the Fourier transforms in radial shells from the center of each transform outwards. Both unweighted phase differences and phase differences weighted by the average of the pairs of normalized amplitudes from each of the Fourier transforms were calculated. Similar measures were calculated in two dimensions using 2D central sections of 3D Fourier transforms, which correspond to 2D projections of the 3D reconstructions. Results were displayed as the cosine of the phase difference with respect to spatial frequency or equivalent resolution. This cosine is a measure of the overlap between the reconstructions at each spatial frequency, determined by

$$\frac{\int_{0^\circ}^{180^\circ} \sin(\theta - \theta_R)\, d\theta}{\int_{0^\circ}^{180^\circ} \sin(\theta)\, d\theta} = \cos(\theta_R), \quad (1)$$

where the denominator is the integral for the reference structure and is the contribution of the Fourier structure amplitude with phase Θ integrated over a sampling interval (defined as half a wavelength at the given spatial frequency). The numerator refers to the structure being compared, and is the contribution of the structure amplitude shifted in phase by Θ_R (the phase difference or phase residual) integrated over the same sampling interval. The ratio is the fractional overlap.

Wire-mesh and solid representations of reconstructions were generated via the program SGI-Expolorer (Sack, 1988). Visualization of reconstructions was on an SGI 4D440 VGX (Silicon Graphics Computer Systems, Mountain View, CA). All reconstructions are shown at an 84% (intensity based) contour level, a threshold which corresponds to the calculated volume of a 54-kDa protein, assuming a protein density of 1.3 g/cm^3. Grid lines in wire-mesh representations of structures are drawn at 5-Å intervals.

For comparisons of other macromolecules with SRP54, crystallographic coordinates of EF-Tu, p21-Ras, and NMR-determined coordinates for calmodulin (La Cour *et al.*, 1985; De Vos *et al.*, 1988; Ikura *et al.*, 1992; coordinates via Protein Data Bank accession codes 1etu, 4q21, and 2bbm, respectively, from the Brookhaven National Laboratory (Upton, NY); Bernstein *et al.*, 1977) were fitted into the SRP54 electron density using the RSR RIGID routine in the program O (Jones *et al.*, 1991). The fit of each structure was refined until no further translational or rotational adjustments in alignment were calculated by the program. Wire mesh representations with cartoon renderings of crystallographic co-ordinates of the protein backbones were generated using the program O.

Amino acid sequence analyses. Sequence alignments were carried out using the local homology algorithm of Smith and Waterman (1981) as encoded in the BESTFIT routine of the Genetics Computer Group Sequence Analysis Software Package Version 7.2. Alignments were carried out on a Vax WorkStation 3100 M38 (Digital Equipment Corporation, Maynard, MA). Similarity calculations were based on the evolutionary distance between the amino acids as described in Gribskov and Burgess (1986).

RESULTS

SRP54 Structure

Purified molecules of SRP54 deposited on thin carbon films, along with particles of TMV as mass standard, were prepared for electron microscopy by quick-freezing and freeze-drying and then examined at liquid nitrogen temperatures at low doses in the Brookhaven STEM. To increase the signal to noise ratio for a given dose the high- and low-angle detector signals of the STEM were combined. A representative field of view of SRP54 molecules and a TMV particle is shown in Fig. 1A. A nonexhaustive selection of images of SRP54 molecules is indicated by the square fields. These images were selected automatically on the basis of size and molecular weight (Andrews *et al.*, 1986). A number of such structures are shown enlarged in Fig. 1B.

The molecular weights for 200 selected particles, using TMV as a mass standard, are shown as the histogram in Fig. 1C. The average is 46 kDa. The observed variation of values is typical for mass measurements by STEM (Wall and Hainfeld, 1986). As expected from low-dose STEM images taken at low temperature, the mass loss is small; the average mass discrepancy from the ideal of 54 kDa can for the most part be accounted for by loss through volatilization of constituent hydrogen atoms. Such atoms cannot be rendered nonvolatile even at liquid nitrogen temperatures.

The relative orientations of sets of molecular images of SRP54 were determined first using sinogram correlation functions and geometric approaches. Optimization among orientation assignments, necessary due to noise in the images, was then carried out using quaternion vector mathematics (Farrow and Ottensmeyer, 1992). In this optimization process, subsets of no more than 5 to 8 randomly selected images were required to fix the best orientation of any given image. To determine the reproducibility of the structural characteristics, a set of 200 molec-

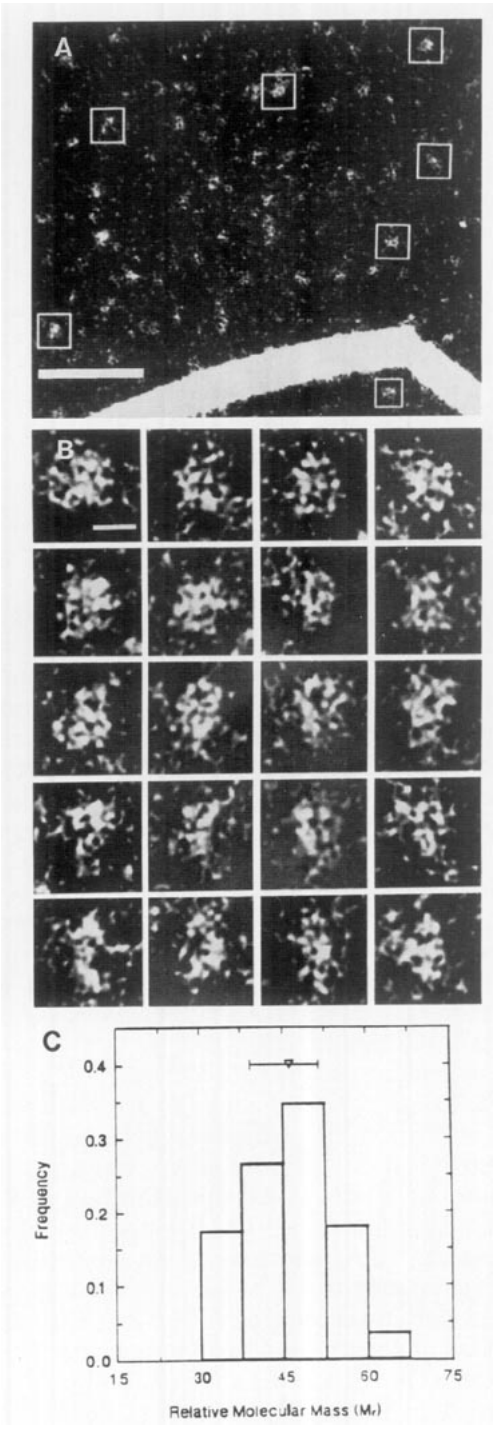

FIG. 1. Scanning transmission electron microscope (STEM) images and mass measurements of SRP54. (A) Digitally recorded micrograph (512 × 512 pixels) of SRP54 molecules at a measured signal to noise ratio of 6.3. Boxes indicate only a few representative examples of the molecules of SRP54 in the field selected on the basis of mass and size. Tobacco mosaic virus used as an internal mass standard is shown in the lower right. Scale bar, 500 Å. (B) A representative gallery of SRP54 molecules selected using molecular mass as a criterion. Images have been contrast enhanced for purposes of presentation. Scale bar indicates 50 Å. (C) Histogram of calculated masses for 200 automatically selected SRP54 molecules. Horizontal bars extend from the median (indicated via a triangle) to upper and lower quartiles.

ular images was arbitrarily divided into two sets of 100 from which reconstructions were calculated independently, along with the reconstruction from the set of the 200 images. The image orientations calculated, and plotted in Fig. 2A, indicate a random distribution of angles for one set of 100 images. Similarly random distributions were obtained from the other image set.

The three-dimensional reconstructions from the three sets of images are shown in Figs. 2B to 2D, presented at a threshold which corresponds to the volume of the 54-kDa molecular weight of SRP54. A major concordance in structure is seen between the reconstructions from the sets of 100 independent images (Figs. 2B and 2D) as well as between these structures and the reconstruction from the total 200 images (Fig. 2C). The latter concordance might be expected *a priori;* however, the orientations for the 200 image reconstruction are in fact completely independent determinations and optimizations of angles among newly and randomly chosen small subsets of images (Farrow and Ottensmeyer, 1992). The result in principle is a third independent 3D reconstruction.

A solid representation of the 200-image reconstruction is shown in Fig. 3 at two orientations related by a 180° rotation. Figure 3A indicates that the structure is divided into two domains of unequal size. The larger domain, roughly triangular or wedge-shaped, comprises about 60% of the mass (right, labeled "W"), while the remaining mass forms a smaller crescent-shaped domain "C" and a slender bridge "B" (Fig. 3B) joined to the wedge-shaped domain on one side of the molecule.

Resolution

The structure of SRP54 has not been obtained by other techniques, preventing a direct comparison of this 3D reconstruction with a known archetype for the protein. Direct measurements between reproducible, separable features in the structures, such as the linker and the crescent-shaped domain, suggest a resolution just better than 15 Å. A better, objective measure of the resolution and consistency in structure can be obtained by phase analysis of the 3D Fourier transforms of the three calculated reconstructions after their translational and rotational alignment in three dimensions. The calculated phase at any spatial frequency in the 3D Fourier spectrum of the molecule represents the positioning of the density variations in the structure at that level of detail. A phase difference, or phase residual, of 0° for identical spatial frequencies from two aligned molecules means exact overlap of structure, while a phase difference of 90° represents complete randomness, i.e., the noise limit, between the structure at this level of detail. The spatial frequency at

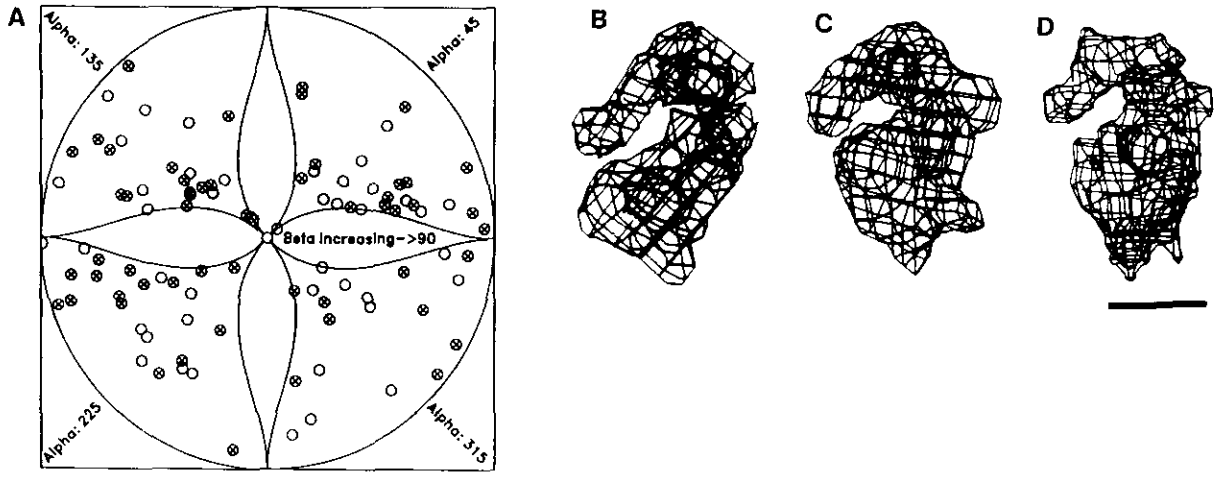

FIG. 2. Calculated molecular orientations and comparison of independent 3D reconstructions of SRP54. (A) Calculated relative angular orientations for individual molecular images in terms of their first two Euler angles (α,β) for the 3D reconstruction shown in Fig. 2B. The first two Euler angles for each image are shown in a cartographic representation of points on the surface of a sphere (Farrow and Ottensmeyer, 1993). Open circles represent orientations on the top half of the sphere (Euler angle β less than or equal to 90°), circles with crosses represent orientations on the bottom half (Euler angle β greater then 90°). (B–D) Reconstructions computed from individual sets of 100, 200, and 100 automatically selected images. The 100-image reconstructions are independent. The 200-image reconstruction is an independent calculation using all images. Scale bar, 25 Å.

which on average a phase difference of 90° first occurs has been taken as a measure of the resolution limit in 3D reconstructions (Stewart *et al.*, 1991; Crowther, 1971). Although more conservative arbitrary cut-offs, such as 45 or 60°, have been used as well for the resolution limit, a separate measure, the Fourier ring correlation at the noise limit between two structures, has produced the same resolution limit as the noise-limited 90° phase residual (Frank *et al.*, 1986).

As a more intuitive representation of the phase residual approach, the cosine of the phase difference is a measure of the integrated overlap of the structure at each spatial frequency (see Materials and

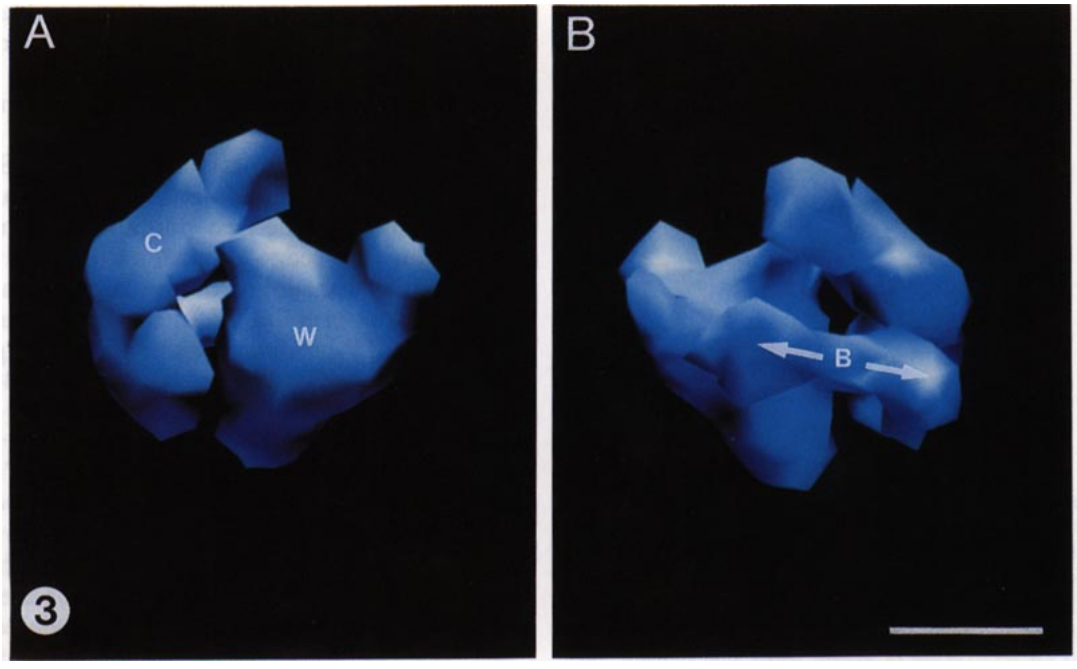

FIG. 3. Two views of the SRP54 reconstruction computed from 200 images at orientations depicting prominent features. (A) View showing crescent domain (labeled C) and wedge-shaped domain (labeled W). (B) Orientation showing bridge (labeled B). The view in B is related to A by a 180° rotation about a vertical axis through the center of the molecule. The crescent-shaped domain in A is related in position to the top part of the reconstructions in Figs. 2B to 2D by a rotation of 90° in the plane of the image and by an additional tilt of about 45°. Scale bar, 25 Å.

Methods for derivation), with 1.0 being complete overlap (phase difference equal to zero), 0.0 no overlap (phase difference 90°), and negative values indicative of a negative structural correlation. Figure 4 indicates the resolution limits using this overlap criterion as calculated in pair-wise comparisons between the reconstructions. Since different arbitrary definitions for the limits are used in the literature, the full curves are given here. The comparison between the two independent 100-image reconstructions indicated a similarity in 3D structure up to a limit of 14.9 Å (no overlap of structure), while this limit between the 200-image reconstruction and each of the 100-image reconstructions had an average value of 12.4 Å (12.8 and 11.4 Å). These values are close to the theoretical resolution limit of 10 Å based on the Shannon sampling theorem (Shannon, 1949), since the original images were acquired with a 5 Å pixel size.

The curves in Fig. 4 decrease to a 50% value in overlap of structural detail at about 30 and 23 Å and then have a shoulder to the 15- to 12-Å limits, respectively. The shoulder can be interpreted as an indication of higher resolution at some orientations within the structure averaged with other orientations at lower resolution. This interpretation is in part borne out by the analysis of central sections of the 3D Fourier volume, which are equivalent to 2D projections of the 3D structures at specific orientations. Several of these 2D projections were sufficiently similar between the reconstructions to show correlation of detail even at the theoretical resolution limit (phase difference of only 79° at 10 Å; Fig. 4). Others did not.

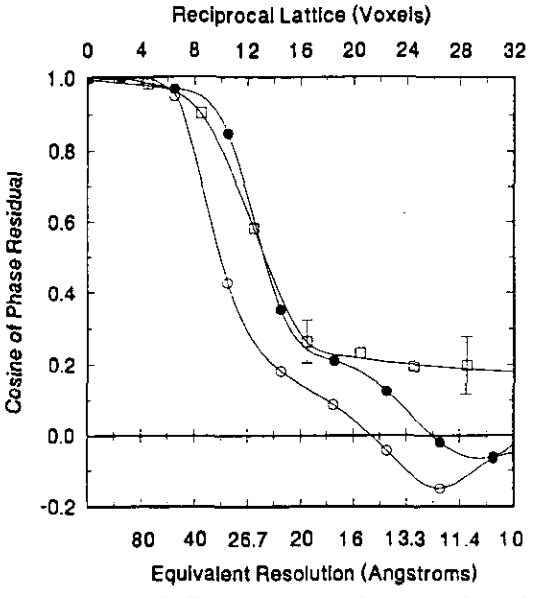

FIG. 4. Results of 3D Fourier transform based resolution analyses. The cosine of the phase residual averaged within spherical shells is given as a function of the radius in voxels (top) or in equivalent resolution in angstoms (bottom). Solid dots indicate the averaged results of analyses between the 200-image reconstruction and each of the two 100-image reconstructions, with a limit at 12.4 Å for no overlap in detail. Open dots indicate the results of the analysis between the two 100-image reconstructions, with a limit of 14.9 Å. Open squares are averaged results for a number of central sections of the 3D Fourier transform in which the cosine of the phase difference was always positive, i.e., the resolution was limited only by the pixel size (Shannon, 1949).

Weighting of the phase differences by the corresponding amplitudes in the Fourier transform had little effect on the outcome, in the first comparison above leaving the 12.4 Å resolution limit unchanged, reducing the resolution of 14.9 to 15.7 Å in the second, and improving the phase difference in the central sections from 79 to 76°.

Irrespective of resolution the overall 3D correlation coefficient was calculated to be 0.80 between the two 100-image reconstructions and 0.85 and 0.82 between the two 100-image 3D structures and the 200-image reconstruction (between the 3D structures represented in Figs. 2B and 2D and Fig. 2C, respectively).

Structural Correlation with Related Molecules

SRP54 function involves the binding of GTP, hydrolysis of this moiety, and release of GDP, as well as the monitoring, binding, and release of the nascent polypeptide signal sequence. The structural resolution of the current reconstruction is not sufficient *a priori* for detailed modeling in terms of function. However, a number of proteins of known structure have domains with functions and amino acid sequences similar to those of SRP54. The results of a structural comparison between three of these proteins and the domains of the SRP54 structure are presented below.

The genetic and functional division of SRP54 into a larger GTP-binding domain (G-domain) and a smaller methionine-rich domain (M-domain) suggests that the wedge-shaped, more massive domain in the SRP54 model structure represents the G-domain of this protein. A functionally related structure, the GTP-binding domain of the elongation factor EF-Tu of *Micrococcus luteus* has a 46% amino acid similarity (20% identity) with the G-domain of SRP54 (Table I). This degree of similarity and of identity is the same as that between EF-Tu and p21-RAS (Table I), two proteins which are known to have a close resemblence in their crystallographic tertiary structure (Berchtold *et al.*, 1993). The electron density of the GTP-binding domain of the crystallographic structure of EF-Tu was modeled into the envelope of the wedge-shaped domain of the SRP54 structure and optimized in placement with respect to the calculated SRP54 densities using crystallographic refinement algorithms. The results, with a peptide backbone representation of EF-Tu, are

TABLE I
Sequence Analyses

Comparisons			% Similarity	% Identity
SRP54 N-terminus (52–268)[a]	vs	p21 (1–189)	47	18
SRP54 N-terminus (4–295)	vs	EF-Tu (57–394)	46	20
p21 (1–189)	vs	EF-Tu (10–231)	45	22
SRP54 C-terminus (425–500)	vs	Calmodulin (71–147)	49	18

[a] Numbers in parentheses refer to matched sequences of amino acid residues used for homology determination.

shown in stereo views in Figs. 5B and 5C at two different orientations. The fit is satisfyingly close in spite of the 54% dissimilarity in amino acid sequence, with the surfaces of the two molecules being virtually coincident on every facet. Only a few parts of the secondary structure elements of EF-Tu break the surface of the SRP54 reconstruction. One helix of EF-Tu extends into the bulb-like end of the linker region on the wedge-shaped domain (cf. Figs. 5C and 3B), suggesting a firmer association between the domain and this part of the linker.

A similar procedure was used to test the fit of the G-protein p21-RAS, which has a 45% similarity (18% identity) with the G-domain of SRP54 (Table I). Again, the fit was very close in overall shape, although not as good as for the EF-Tu domain, a beta-sheet/loop region noticeably extending about 5 Å outside the surface of the SRP54 domain (Fig. 5E). At the same time the surfaces of p21-RAS are generally inside the boundaries of the SRP54 structure, likely as a consequence of the smaller size of p21-RAS in relation to the wedge-shaped domain of the SRP54 structure (21 kDa versus about 32 kDa, respectively).

Also shown in Figs. 5B and 5E are the locations of the binding sites of the guanine nucleotides (GDP form) in EF-Tu and p21-RAS. In both instances GDP at these sites juts into the gap between the wedge-shaped and crescent-shaped domains of SRP54 and faces the bottom portion of the inside of the crescent-shaped domain. This result may be significant, since, during the fitting of the crystal structures of the two molecules into the wedge-shaped domain of SRP54, no consideration was given to the locations of these binding sites.

The M-domain of SRP54 and the regulatory protein calmodulin share the general property of binding to peptide sequences (Zopf *et al.*, 1990; O'Neil and DeGrado, 1990; O'Neil *et al.*, 1989). In the calmodulin structure methionine-containing hydrophobic pockets are responsible for binding to hydrophobic helical peptide regions (Babu *et al.*, 1988; Ikura *et al.*, 1992). An analogy in structure/function relationship between calmodulin and SRP54 has been suggested, based on the presence of such methionine-containing regions in both molecules (Zopf *et al.*, 1990). Sequence comparison of these regions indicated a 49% similarity (18% identity) over the last 80 amino acids of the C-terminal of both proteins (Table I). Moreover, the methionine-containing clusters occur at comparable separations in the sequences of these regions (Table II). While such levels of similarities cannot point to secondary and tertiary folding similarities with certainty, they are sufficiently suggestive to make a 3D structural comparison of interest. This region of the structure of calmodulin (Ikura *et al.*, 1992) was modeled as linked amino acids into the crescent-shaped domain of the calculated SRP54 structure (Fig. 5D). Similarities in structure were observed, with the elbow shape of the calmodulin structure fitting well into the bend of the crescent of SRP54. However, since this region of calmodulin has a molecular weight of only 10 kDa compared to a mass equivalent to about 15 kDa for the SRP54 crescent domain (with about 5 kDa in the linker), some of the SRP54 domain cannot be and is not filled by the calmodulin sequence. This is most noticeable in the upper portion of the elbow in Fig. 5D.

DISCUSSION

The 3D reconstructions of the SRP54 structure have indicated a number of features that not only indicate internal consistencies of detail, but also concur with structural characteristics of proteins with domains exhibiting similar amino acid sequences and related functions. The structural and functional properties are examined below.

Resolution Potential

The reconstructions of the SRP54 structure carried out from low-dose STEM dark-field micrographs of randomly oriented molecules examined at low temperature indicate a reproducible level of structural detail near 15 Å, close to the limit of 10 Å, which for the present digital image acquisition using 5-Å pixels is the theoretical resolution given by the Shannon sampling theorem (Shannon, 1949). This result has to be examined from at least two aspects, imaging capability and radiation dose.

Typical resolutions in bright field are limited in general to between 20 and 30 Å by the size of the heavy atom contrast agents or by the normal defocus effect on the contrast transfer function of the microscope for both stained and unstained frozen-hydrated specimens. Only defocus correction of the contrast transfer function combined with the signal averaging possible in 2D crystals has so far resulted in major improvements over these limits (Unwin

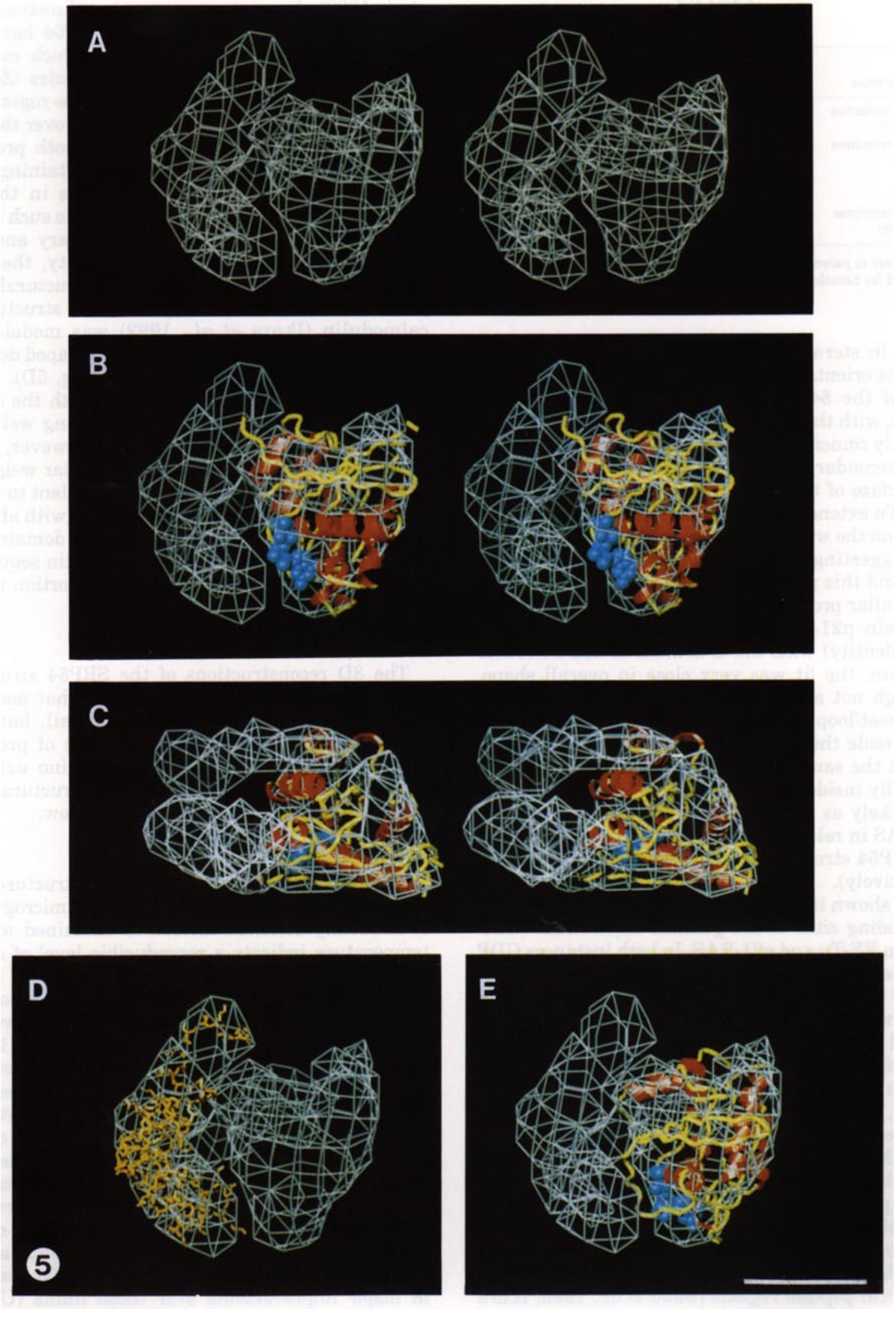
A
B
C
D
E
5

TABLE II
The Relative Incidence and Positions of Methionine Rich Clusters in SRP54 and Calmodulin[a]

SRP54	Calmodulin
1	0, 1
5, 17, 26, 33	5
36, 37, 45, 48	37
54, 55, 66	52
69, 70	72, 73

[a] Numbers indicate relative positions of methionine clusters in the SRP54 M-domain (amino acids 425 to 500) and calmodulin (amino acids 71 to 147). The positions of methionines relative to GLN 429 in SRP54 and the positions of methionines in calmodulin relative to MET 72 are summarized, with methionines in similar relative positions identified in **boldface**.

and Henderson, 1976; Henderson *et al.*, 1990; Kühlbrandt *et al.*, 1994). In the STEM dark field the beam size (or pixel size) and the radiation dose are the limiting factors, since the contrast transfer function for this instrument is always positive right to the beam size resolution limit (Hillyard *et al.*, 1993). For the current work the STEM beam size was smaller than the 5-Å pixel size used for image acquisition, making the latter the theoretical limiting factor.

However, since the dose in each individual micrograph was about 25 e/Å^2, the resolution must also be examined in the light of data acquired by other electron microscopic techniques at various radiation doses. Data on 2D crystals used for 3D reconstruction is frequently obtained at a dose of 10 e/Å^2 (Gogol *et al.*, 1989). However, the most stringent criterion, a "critical dose" measured by the fading of diffraction in 2D crystals to about one-third of the original intensity, demands a dose as low as 0.5 e/Å^2 at room temperature (Unwin and Henderson, 1976). Crystal-diffraction fading evaluates the perfection of long-range lateral alignment of molecules, a very sensitive measure not only of molecular damage as the result of irradiation, but also of even slight rotations or shifts of molecules which are otherwise undamaged. Thus fading of diffraction is a measure of overall loss of crystallinity, not just of molecular damage.

A different measure of radiation damage is the integrity of the chemical structure of a molecule as measured by the molecular absorption in thin molecular films using electron energy loss spectroscopy (Isaacson *et al.*, 1973). This technique determined critical doses for loss of the molecular absorption signal to be 10 to 100 e/Å^2 at room temperature, with the higher values belonging to compounds with a greater degree of aromaticity. Furthermore, these authors calculated that at a dose of 10 e/Å^2 a spatial resolution of 10 Å is possible in STEM.

At liquid nitrogen temperatures, measurements on 2D crystals have indicated critical doses of 10 e/Å^2 for resolutions of 10 Å, doses about five times higher than at room temperature (Hayward and Glaeser, 1979). In addition, using statistical arguments, Hayward and Glaeser (1979) calculated that the optimal dose for imaging should be 2.5 times this value. Combining the 10 e/Å^2 critical dose in crystal diffraction with the factor of 2.5 for optimal imaging one arrives at a dose of 25 e/Å^2, the dose used to obtain the present results.

Damage to individual molecules in projection has been more difficult to quantify. However, an extended study on imaging of protamine, a 4-kDa protein, with doses from 60 e/Å^2 in the STEM to 1500 e/Å^2 in the TEM, and dose rates changed by over seven orders of magnitude, indicated that in the STEM at 60 e/Å^2 virtually all protamine molecules still exhibited a characteristic 3- to 5-Å finger-like detail in the images (Ottensmeyer *et al.*, 1978). The spatial resolution seen in these images did not imply that the 3D structure of the molecules remained intact, but merely that at 60 e/Å^2 the mass density of the molecules as projected into the image plane had not spread laterally to such a degree as to obliterate this level of detail. Thus achievement of an irradiation dose much lower than 60 e/Å^2, approaching the equivalent of 0.5 e/Å^2 at room temperature, would be assurance that a 3D reconstruction from images of individual molecules would not be limited in resolution by radiation damage.

If for low-dose irradiation of molecules one assumes that electron quantum noise, variations in carbon support film structure for the molecules, as well as radiation damage in random sites within the molecules can be treated as Poisson events, then averaging of images would reduce their effects in cal-

FIG. 5. Structural correlations of SRP54 and other molecules. (A) Stereo view in parallel projection of wire mesh representation of SRP54, with the linker behind the two domains. (B and C) Wire mesh representation of SRP54 with crystallographic coordinates of the GDP-bound form of EF-Tu computationally fitted into the SRP54 electron density. For clarity the EF-Tu peptide backbone coordinates only are shown as a cartoon with α-helices colored red and β-strands and loops in yellow. Breaks in the EF-Tu crystallographic structure (La Cour *et al.*, 1985) are generated where no coordinates have been assigned during their structure determinations. Blue spheres in both panels demark the location of the bound GDP displayed with radii equal to 0.5 of the van der Waals radii of the constituent atoms. The view in C is related to the view in B by a rotation of 90° about a horizontal axis in the plane of the page such that the front face of the molecule in B forms the bottom edge of the view in C. (D) SRP54 structure with stick representation of calmodulin amino acids 71 to 149 (Ikura *et al.*, 1992) computationally fitted into the crescent-shaped SRP54 domain. (E) SRP54 structure with cartoon representation of p21-RAS and bound GDP (De Vos *et al.*, 1988). Coordinate fitting and color coding is as in B.

culable ways. Thus, averaging 100 images taken at 25 e/Å^2 would produce a composite with a damage level equivalent to that dose reduced by $\sqrt{100}$, or 2.5 e/Å^2. Moreover, since in molecules imaged at liquid nitrogen temperatures the effect of irradiation is reduced further by a factor of about 5 in relation to radiation damage incurred at room temperature (Hayward and Glaeser, 1979), the effective damaging dose in the averaged structure obtained from images of molecules at low temperature would be virtually commensurate with the 0.5 e/Å^2 critical dose of the crystal diffraction fading criterion at room temperature.

Therefore, from combined theoretical and experimental considerations the measured resolution to be expected for the SRP54 reconstructions would be defined by the sampling limit, by other quantum noise effects, and by the number of projections and orientations used rather than by radiation damage. This is a far-reaching deduction, since it implies not only that the near-10-Å resolution observed here is possible, but also that higher resolution reconstructions should be obtainable with a great number and more detailed STEM images used as input to the algorithm. The observation that several 2D projections in the 3D reconstructions have not reached their correlation limit at 10 Å (Fig. 5) is already suggestive of the experimental potential for a resolution beyond this value. However, even at the currently obtained 12- to 15-Å limits in the 3D reconstructions, useful structural correlations can be drawn with genetic, biochemical, and functional data.

Structural Correlation

The two-domain structure for SRP54 reported here is compatible with proteolytic dissection and phylogenetic comparisons which suggest that SRP54 contains two distinct structural domains (Scoulia *et al.*, 1987; Römisch *et al.*, 1989; Bernstein *et al.*, 1989; Zopf *et al.*, 1990). Limited proteolytic digestions of the molecule with either elastase or V8-protease, or of the intact SRP complex with elastase, yield primary products which have molecular weights of 33 and 22 kDa (Scoulia *et al.*, 1987; Zopf *et al.*, 1990). Domain-specific antisera, reconstitution, and cross-linking studies have been used to identify these fragments as the N-terminal GTP-binding and C-terminal methionine-rich domains (G-domain and M-domain), respectively (Zopf *et al.*, 1990; Lütcke *et al.*, 1992). In the 3D reconstruction the wedge-shaped domain accounts for three-fifths of the mass of SRP54, and two-fifths of the mass is accounted for in the crescent-shaped domain and most of the linking bridge. This correspondence suggests that they are the G- and M-domains, respectively. Moreover, the apparent accessibility of the bridge connecting the two structural domains (Fig. 3B) suggests a ready site for enzymatic cleavage into two asymmetric fragments of the biochemically observed size. Sequence analyses indicate relatively high homology of the amino-terminal region of SRP54 with the GTP-binding domain of EF-Tu and with p21-RAS (Table I), as well as the presence of a GTP-binding consensus sequence in the three molecules (Römisch *et al.*, 1989; Bernstein *et al.*, 1989) (Fig. 6). With our suggested structural assignment of the wedge-shaped domain of SRP54 to the N-terminal region of the molecule, it is satisfying that the overall size and shape of this wedge-shaped domain correspond to dimensions and features present in crystallographic structures for GTP-binding proteins such as EF-Tu or p21-RAS (La Cour *et al.*, 1985; De Vos *et al.*, 1988). Fine dissimilarities, such as the absence of matching mass in the small extension of the posterior upper lobe of the wedge-shaped domain (Fig. 5B), could be due to amino acid differences, but they are too detailed to be usefully considered at this point. Differences in structure observed are no greater than those between EF-Tu and p21-RAS, which have amino acid sequences with as similar a degree of homology between them as they do with respect to SRP54 (Table I).

The M-domain of SRP54 has been shown to contain binding sites for SRP RNA and for secretory signal sequences (Kurzchalia *et al.*, 1986; Krieg *et al.*, 1986; Zopf *et al.*, 1990; Römisch *et al.*, 1990; High *et al.*, 1991; Samuelsson and Olsson, 1993). It has been proposed that the methionines in this domain form a flexible hydrophobic pocket that accommodates relatively heterogeneous secretory signal se-

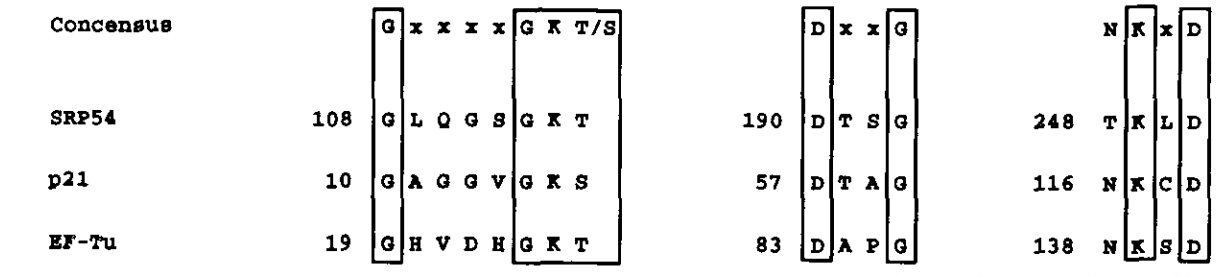

FIG. 6. The three consensus sequence elements for a GTP-binding domain as present in SRP54 (Dog), p21 (H-ras-1; Human), and EF-Tu (*M. luteus*). Numbers in front of the sequence motifs refer to amino acid positions in each protein. Adapted from Römisch *et al.* (1989).

quences, binding to the hydrophobic core of the signal akin to the binding of hydrophobic α-helices by calmodulin (Bernstein *et al.*, 1989; Zopf *et al.*, 1990; Ikura *et al.*, 1992). In the amino acid sequence of calmodulin from residues 71 to 149, seven methionines form four well-separated methionine regions among hydrophobic residues on the interior side of its elbow-like structure (Ikura *et al.*, 1992). Analogously, the M-domain of SRP54 has four methionine-rich hydrophobic clusters at corresponding separations (Table II), which include 13 methionine moieties in general either adjacent in a cluster or separated by the equivalent of one or two α-helical turns. In this region the SRP54 amino acid sequence has a 49% similarity with the predominantly α-helical calmodulin (Table I), suggestive of similar secondary structure elements. Thus, equivalently, the methionine clusters of SRP54 can be modeled to be on the interior side of the crescent shaped M-domain. This region faces and is in close proximity to the putative G-domain near the GTP-binding site (cf. Figs. 5B, 5D, and 5E).

Structure/Function Hypotheses

The proposed juxtaposition of critical regions in the molecule suggests that the signal sequence peptide would be located in or near the gap between the two structural domains. This physical location would be in agreement with a large number of biochemical observations which have implicated the simultaneous interaction of both the G- and M-domains with the signal sequence. It can provide a natural explanation for the incompatibility between simultaneous binding of the signal sequence and GTP or GDP (Miller *et al.*, 1993). Furthermore, it can explain the decrease in signal-sequence-binding activity observed with mutants in which the G-domain is deleted (Zopf *et al.*, 1993). Moreover, it is compatible with the observation that complete loss of SRP54 function by alkylation of the G-domain cysteine residues is partially relieved by proteolytic removal of the modified SRP54 G-domain (Lütcke *et al.*, 1992). From this biochemical data, from the analysis of the 3D reconstruction, and from the comparisons with GTP-binding and peptide-binding domains of proteins exhibiting homologous sequences and functions one can infer that the location of the signal-sequence binding site is on the interior of the crescent-shaped domain, facing the putative GTP site on the wedge-shaped domain of the structure.

The three-dimensional structure of SRP54 described here suggests a biochemically compatible model for signal-sequence binding in which the M- and G-domains function as a molecular clamp hinged at the connecting bridge. *In vitro* SRP has been shown to bind to cytoplasmic ribosomes in the absence of a nascent secretory signal sequence (Walter *et al.*, 1991); therefore, the SRP54 clamp should be positioned near the nascent-chain exit site of the ribosome *in vivo* where it monitors all newly synthesized polypeptides (secretory or cytoplasmic) emerging from the ribosome. This is consistent with biochemical observations which indicate that nonsecretory nascent polypeptides can be cross-linked to SRP54 (M. Wiedmann, personal communication). Moreover, the efficient SRP-mediated targeting of molecules with internal signal sequences supports this model (Perara and Lingappa, 1985; Simon *et al.*, 1987). The emergence of a secretory signal sequence from the ribosome would trigger a conformational change in SRP54, such as closure of the clamp on the signal sequence. This may be sufficient to account for the observed increase in affinity of SRP for polysomes of nascent secretory proteins (Walter *et al.*, 1991). However, additional SRP-ribosome interactions may be needed for the SRP-mediated arrest or slowing of translation observed upon signal-sequence binding (Wolin and Walter, 1987; Walter *et al.*, 1991). After targeting of the protein-synthetic complex and binding of SRP to its membrane receptor, the receptor promotes a change in SRP54 to a conformation which permits release of the signal sequence concomitant with GTP binding (Miller *et al.*, 1993). Hydrolysis of GTP to a loosely-bound GDP permits release of SRP from the receptor (Zopf *et al.*, 1993; Miller *et al.*, 1993) and restores the conformation required for the monitoring of new signal sequences.

Thus the structure for SRP54 reported here provides a detailed structural framework for the known biochemical observations and furnishes an initial model structure as reference for investigations of conformational changes that occur in the cycle of SRP54 function. Such conformational changes, even if smaller than those seen between the GTP and GDP forms of EF-Tu (Kjeldgaard *et al.*, 1993), should be observable using the current 3D reconstruction approaches on purified SRP54 complexed with its natural ligands or with ligand analogues.

We thank Peter Walter for his generous gift of the purified SRP54 used to initiate this project, George Harauz for use of his set of IMAGIC programs, and Joseph Wall and colleagues for use of the Brookhaven National Laboratory electron microscope facilities. We especially thank Brenda Rutherford for excellent technical assistance. We thank André White for introduction and assistance with the program O. G.J.C. is a recipient of a Connaught scholarship. The work was supported by grants from the Medical Research Council of Canada, the National Cancer Institute of Canada, and by funds from the Ontario Cancer Treatment and Research Foundation.

REFERENCES

Andrews, D. W., Walter, P., and Ottensmeyer, F. P. (1985) *Proc. Natl. Acad. Sci. USA* 82, 785–789.

Andrews, D. W., Yu, A. H. C., and Ottensmeyer, F. P. (1986) *Ultramicroscopy* 19, 1–14.

Andrews, D. W., Walter, P., and Ottensmeyer, F. P. (1987) *EMBO J.* 6, 3471–3477.

Babu, Y. S., Bugg, C. E., and Cook, W. J. (1988) *J. Mol. Biol.* **204**, 191–204.

Berchtold, H., Reshetnikova, L., Reiser, C. O. A., Schirmer, N. K., Sprinzl, M., and Hilgenfeld, R. (1993) *Nature* **365**, 126–132.

Bernstein, F. C., Koetzle, T. F., Williams, G. J. B., Meyer, E. F., Jr., Brice, M. D., Rodgers, J. R., Kennard, O., Shimanouchi, T., and Tasumi, M. (1977) *J. Mol. Biol.* **112**, 535–542.

Bernstein, H. D., Poritz, M. A., Strub, K., Huben, P. J., Brenner, S., and Walter, P. (1989) *Nature* **340**, 482–486.

Crowther, R. A. (1971) *Phil. Trans. Roy. Soc. Lond.* **B261**, 221–230.

De Vos, A. M., Tong, L., Milburn, M. V., Matias, P. M., Jancarik, J., Noguchi, S., Nishimura, S., Miura, K., Ohtsuka, E., and Kim, S. (1988) *Science* **239**, 888–893.

Farrow, N. A., and Ottensmeyer, F. P. (1992) *J. Opt. Soc. Am.* **A9**, 1749–1760.

Farrow, N. A., and Ottensmeyer, F. P. (1993) *Ultramicroscopy* **52**, 141–156.

Frank, J., Radermacher, M., Wagenknecht, T., and Verschoor, A. (1986) *Ann. N. Y. Acad. Sci.* **483**, 77–87.

Frank, J., Carazo, J.-M., and Radermacher, M. (1988) *Eur. J. Cell Biol.* **48**, 143–146.

Gilmore, R., Blobel, G., and Walter, P. (1982a) *J. Cell Biol.* **95**, 463–469.

Gilmore, R., Walter, P., and Blobel, G. (1982b) *J. Cell Biol.* **95**, 470–477.

Gogol, E. P., Lücken, U., Bork, T., and Capaldi, R. A. (1989) *Biochemistry* **28**, 4709–4716.

Gribskov, M., and Burgess, R. R. (1986) *Nucleic Acids Res.* **14**, 6745–6763.

Hayward, S. B., and Glaeser, R. M. (1979) *Ultramicroscopy* **4**, 201–210.

Henderson, R., Baldwin, J. M., Ceska, T. A., Zemlin, F., Beckmann, E., and Downing, K. H. (1990) *J. Mol. Biol.* **213**, 899–929.

High, S., and Dobberstein, B. (1991) *J. Cell Biol.* **113**, 229–233.

Hillyard, S., Loane, R. F., and Silcox, J. (1993) *Ultramicroscopy* **49**, 14–25.

Ikura, M., Clore, G. M., Gronenborn, A. M., Zhu, G., Klee, C. B., and Bax, A. (1992) *Science* **256**, 632–638.

Isaacson, M., Johnson, D., and Crewe, A. V. (1973) *Radiat. Res.* **55**, 205–224.

Jones, T. A., Zoum, J. Y., Cowan, S. W., and Kjeldgaard, M. (1991) *Acta. Crystallogr.* **A47**, 110–119.

Kjeldgaard, M., Nissen, P., Thirup, S., and Nyborg, J. (1993) *Structure* **1**, 35–50.

Krieg, U. C., Walter, P., and Johnson, A. E. (1986) *Proc. Natl. Acad. Sci. USA* **83**, 8609–8608.

Kühlbrandt, W., Wang, D. N., and Fujiyoshi, Y. (1994) *Nature* **367**, 614–621.

Kurzchalia, T. V., Wiedmann, M., Girskovich, A. S., Bochkareva, E. S., Bielka, M., and Rapoport, T. A. (1986) *Nature* **320**, 634–636.

La Cour, T. F. H., Nyborg, J., Thirup, S., and Clark, B. F. C. (1985) *EMBO J.* **9**, 2385–2388.

Lütcke, H., High, S., Römisch, K., Ashford, A. J., and Dobberstein, B. (1992) *EMBO J.* **11**, 1543–1551.

Meyer, D. I., Krause, E., and Dobberstein, B. (1982) *Nature* **297**, 647–650.

Miller, J. D., Wilhelm, H., Gierasch, L., Gilmore, R., and Walter, P. (1993) *Nature* **366**, 351–354.

O'Neil, K. T., Erickson-Viitanen, S., Wolfe, H. R., Jr., and DeGrado, W. F. (1989) *J. Biol. Chem.* **264**, 14571–14578.

O'Neil, K. T., and DeGrado, W. F. (1990) *Trends Biochem. Sci.* **15**, 59–64.

Ottensmeyer, F. P., Bazett-Jones, D. P., Rust, H. P., Weiss, K., Zemlin, F., and Engel, A. (1978) *Ultramicroscopy* **3**, 191–202.

Ottensmeyer, F. P., and Farrow, N. A. (1992) *Proc. Elect. Microsc. Soc. Am.* **50**, 1058–1059.

Penchek, P., Radermacher, M., and Frank, J. (1992) *Ultramicroscopy* **40**, 33–53.

Perara, E., and Lingappa, V. R. (1985) *J. Cell Biol.* **101**, 2292–2301.

Radermacher, M. (1994) *Ultramicroscopy* **53**, 121–136.

Radermacher, M., Wagenknecht, T., Verschoor, A., and Frank, J. (1987) *J. Microsc.* **146**, 113–122.

Römisch, K., Webb, J., Herz, J., Prehn, S., Frank, M., Vingron, M., and Dobberstein, B. (1989) *Nature* **340**, 478–482.

Römisch, K., Webb, J., Lingelbach, K., Gausepohl, H., and Dobberstein, B. (1990) *J. Cell Biol.* **111**, 1793–1802.

Sack, J. S. (1988) *J. Mol. Graphics* **6**, 224–225.

Samuelsson, T., and Olsson, M. (1993) *Nucleic Acids Res.* **21**, 847–853.

Scoulia, E., Krause, E., Meese, K., and Dobberstein, B. (1987) *Eur. J. Biochem.* **163**, 519–528.

Shannon, C. E. (1949) *Proc. Inst. Radio Eng.* **37**, 10–21.

Siegel, V., and Walter, P. (1985) *J. Cell Biol.* **100**, 1913–1921.

Siegel, V., and Walter, P. (1988) *Cell* **52**, 39–49.

Simon, K., Perara, E., and Lingappa, V. R. (1987) *J. Cell Biol.* **104**, 1165–1172.

Smith, T. F., and Waterman, M. S. (1981) *Adv. Appl. Math.* **2**, 482–489.

Stewart, P. L., Burnett, R. M., Cyrklaff, M., and Fuller, S. D. (1991) *Cell* **67**, 145–154.

Stewart, P. L., Fuller, S. D., and Burnett, R. M. (1993) *EMBO J.* **12**, 2589–2600.

Unwin, P. N. T., and Henderson, R. (1976) *J. Mol. Biol.* **94**, 425–440.

Unwin, N. (1993) *J. Mol. Biol.* **229**, 1101–1124.

van Heel, M. (1987) *Ultramicroscopy* **21**, 111–124.

Wall, J., and Hainfeld, J., (1986) *J. Annu. Rev. Biophys. Biophys. Chem.* **15**, 335–376.

Walter, P., and Blobel, G. (1983) *Cell* **34**, 525–533.

Walter, P., Ibrahimi, I., and Blobel, G. (1991) *J. Cell Biol.* **91**, 545–550.

Walter, P., and Lingappa, V. R. (1986) *Annu. Rev. Cell Biol.* **2**, 499–516.

Wolin, S. L., and Walter, P. (1987) *EMBO J.* **7**, 3559–3569.

Zopf, D., Bernstein, H. D., Johnson, A. E., and Walter, P. (1990) *EMBO J.* **9**, 4511–4517.

Zopf, D., Bernstein, H. D., and Walter, P. (1993) *J. Cell Biol.* **120**, 1131–1121.